Embedding ultrasonic transducers in concrete: a lifelong monitoring technology

Arnaud Deraemaeker[a,*], Cédric Dumoulin[a,**]

[a] *Université libre de Bruxelles (ULB), École polytechnique de Bruxelles, Building, Architecture and Town Planning department (BATir)*

Abstract

This paper deals with lifelong monitoring of concrete structures using embedded piezoelectric transducers. Thanks to such transducers, monitoring of the concrete can be automated both at the early age, right after the concrete is cast, and over the long term, until the end of the lifetime of the structure. For long term monitoring, the wave velocity variations introduced by operational factors effects should be filtered out. In the present study, we introduce a new technique called the Direct Wave Interferometry (DWI) which uses time stretching only on the early part of the recorded wave. This appears to be a good tradeoff between the high resolution of the Coda Wave Interferometry (CWI) for low velocity variations and the reliability of the measurement of the time of flight (TOF) for large velocity variations.

Keywords: Ultrasonic Wave, Embedded Piezoelectric Transducer, Direct Wave Interferometry (DWI), Concrete Assessment, In-situ Monitoring

1. Introduction

Concrete is the most widely used construction material in the world. It is a complex material whose mechanical properties evolve continuously from the time of casting until the end of its lifetime. During the construction phase, the main issue for the operator is to determine the time when the formworks can be removed which depends mainly on the evolution of the compressive strength. The time when post-tensioning can be applied is also governed by the evolution of the compressive strength. Nowadays, such evolution is assessed through very conservative norms or compressive tests on small specimen which have been cast at the same time as the structure and stored at the same location. There is a certain degree of inaccuracy associated to this technique as the temperature evolution in the actual structure is not the same as the one in small specimens, especially when the structure is massive. In order to overcome this drawback, maturity

*Principal Corresponding Author
**Corresponding Author
Email addresses: aderaema@ulb.ac.be (Arnaud Deraemaeker), cedumoul@ulb.ac.be (Cédric Dumoulin)
URL: batir.ulb.ac.be (Arnaud Deraemaeker)

methods [1, 2] which are based on the measurement of the actual temperature evolution inside the concrete, calibrated laboratory compressive tests on small specimen and the knowledge of the activation energy can be used to get a more accurate estimation of the compressive strength. There exist currently automated maturity systems which allow to monitor remotely and wirelessly the evolution of the compressive strength. There is a clear demand from the industry for such automated solutions. The method does not allow however to estimate the Young's modulus of concrete, which can be of interest at early-age for structures with cantilevers.

Over the time, when the structure is in service, the mechanical properties of concrete can also deteriorate due to several mechanisms such as the loss of prestress in prestressed concrete or chemical attacks such as alkali-silica reactions or delayed ettringite formation. In order to ensure the safety of the infrastructure, it is important to be able to assess its remaining strength. Destructive compressive tests can be performed on sampled cores extracted from the structure. For obvious reasons however, non-destructive techniques are preferable. Among these, the ultrasonic pulse velocity method (UPV) is currently one of the most widely used techniques. It is an established technique described in different national norms among which the European standard *EN 12504-4* [3] or the ASTM norm *C 597 – 02* [4], and used in many commercial systems. It consists in exciting the emitter by a short pulse signal and measuring the time of propagation of the wave from the emitter to the receiver. Knowing the distance between the transducers, the velocity of the fastest wave (the compressive wave, also called the *P*-wave) can be measured. The *P*-wave velocity is related to the mechanical properties (Young's modulus and Poisson's ratio) of the concrete and can therefore be used to assess the uniformity and relative quality of concrete [5]. It can also indicate the presence of voids and cracks [6] and can be used to evaluate the setting time in fresh concrete [7]. Provided an assumption is made on the value of the Poisson's ratio, it can be used to give an estimate of the Young's modulus. The wave velocity has also been shown to be correlated to the concrete compressive strength, but as this relationship depends on many parameters of the concrete, a calibration curve needs to be established for a specific concrete [8].

The typical frequency range for UPV testing is from 20kHz to 200 kHz. In that frequency range, wave propagation in concrete is a complex phenomenon due to the high heterogeneity of the microstructure: the wave sent from the emitter will interact with the aggregates causing multiple reflections. The initial wave will be split in many different components traveling different paths, and reaching the receiver at different times, resulting in a very long recorded signal. Typically, for a pulse input of five microseconds, the signal recorded at the receiver side will be several milliseconds long. Although there is no strict limit, one can distinguish between the early-wave, also called the ballistic wave, and the later wave, called the CODA. The wave components which reach the receiver first have travelled the shortest path, and therefore interacted mainly with the microstructure in the direct line of sight between the emitter and the receiver. The UPV is therefore a measure of the properties of concrete between the emitter and the receiver, while the late arrival wave carries information about more distant locations, but is much more complex to interpret. While still at the stage of re-

search, there have been a few attempts at extracting information from the late CODA. The most widely used technique is coda wave interferometry (CWI) and has been used to estimate the acoustoelastic parameters of concrete in [9, 10]. Providing a dense network of sensors is used, it is also possible to locate damage in a concrete structure using more advanced techniques based on coda wave interferometry [11–13].

There are several drawbacks to the techniques described above. None of them is suited to monitor concrete over the whole lifetime, from the time of casting. Maturity methods are limited to the early age (first few days) and cannot give information about the deterioration of concrete over time or the early cracking. Ultrasonic testing, including UPV and CWI using external probes cannot be used on site at early age due to the presence of formworks, requires manpower and is difficult to apply over the long term due to accessibility issues. Over the last ten years, several researchers have studied the possibility of embedding the ultrasonic probes directly inside the concrete. The first and obvious advantage of the technique is the potential automation of ultrasonic monitoring. Additional advantages are an enhanced coupling (without coupling agents) with the concrete for stronger waves generation over longer paths, the protection of the transducers from environmental and accidental attacks, the possibility to perform measurements in the presence of formworks, and an added flexibility of transducers arrangements which allows for direct wave propagation paths. A major requirement with such transducers is however their low-cost as they will be lost in the structure.

Such kinds of transducers have been successfully used for the monitoring of (i) cement and concrete hydration [14, 15], (ii) the evolution of the compressive strength of concrete at early age [16, 17], (iii) concrete cracking [18–22], (iv) water seepage [23–25] and (v) mechanical properties of concrete [26] including the acoustoelastic effect in compression [27]. At ULB-BATir, we have worked on the development of our own embedded transducers to measure the *P*-wave velocity at early-age [28] and monitor cracking in several laboratory tests [29, 30] (pull-out, three-points bending and compressive tests).

Although limited to laboratory or short-time monitoring, all of these applications show the high potential of ultrasonic testing with embedded transducers to perform real-time on-line monitoring of concrete infrastructure. An important step forward is however needed, as long term monitoring involves environmental variability which needs to be filtered out. It is known that when in service, the temperature, the moisture or the stress state have an impact on the measured ultrasonic signals which needs to be distinguished from the impact of the evolution of the microstructure (damage).

This paper focuses on two important aspects of real-time monitoring: monitoring of the hardening phase of concrete structures, and long-term damage monitoring. For both aspects, the same monitoring hardware is used, which consists in pairs of embedded ultrasonic transducers where the emitter is excited via a pulse excitation, and the signals are recorded at the receiver side. The post-processing is however different for each application: for the hardening phase, automated UPV measurements are performed in order to follow the evolution of the Young's modulus at early age. For the

damage monitoring, a novel method is proposed for the filtering of the environmental effects. It is inspired from the approach used in CWI based on time stretching and the definition of a correlation coefficient, but is applied to the early part of the wave instead of the CODA. The new method, called direct wave interferrometry (DWI) is shown to be better suited for on-line damage monitoring under changing operational conditions. This is because the time stretching method is efficient to remove operational variability only when applied to signals which have travelled through areas in which the stress state, the temperature and the moisture are more or less uniform, which is generally not the case when later parts of the wave are considered. The use of the early wave also preserves the local nature of the damage indicator.

In this paper, the efficiency of the proposed monitoring system based on embedded piezoelectric transducers is demonstrated on two small concrete beams. The test specimens, the embedded transducers and the testing hardware are presented in section 2. The monitoring of the hardening phase and the damage monitoring are presented in sections 3 and 4. The hardening phase is monitored by computing the evolution of the UPV based on the estimation of the time of flight, and deducing the evolution of the Young's modulus. One of the samples is then loaded under a three-point bending test and damage monitoring is performed. The operational variability is due to the evolution of the stress state in the beam which, due to the acoustoelastic effect (change of wave velocity due to the applied stress), impacts the wave velocity even in the absence of damage. The novel approach based on DWI is applied to filter out successfully the acoustoelastic effect. It is also shown that applying time stretching before computing the damage indicator is equivalent to tracking the change of amplitude of the first peak of the recorded waves [30].

2. Specimens and monitoring system

Experiments are performed on two short non-reinforced concrete beams in which a pair of transducers has been embedded with a spacing of 14.3 cm. The beams are made of ordinary concrete. The geometry and the components of the beams are given in Table 1.

The embedded transducers have been developed at ULB-BATir and are made of a thin Lead Zirconate Titanate (PZT) patch which is a piezoelectric material [31, 32] and surrounded by several coating materials (Fig. 1). The use of such embedded transducers allows for direct measurement instead of indirect, semi-direct or through the thickness measurements [31, 33].

The ultrasonic monitoring system is described in Fig. 2. It is composed of a data acquisition board NI PXI-6115 ($10 MHz$ sampling rate) and a variable gain pre-amplifier SmartPre ($+18 - 60\ dB$, band-pass $1\ kHz - 1 MHz$) designed by SMARTMOTE which are controlled by an in-house program based on the LabView programming environment. The system is able to perform up to 150 ultrasonic measurements per second while the signal which is generated is a short pulse of $5\mu s$ corresponding to a frequency band up to 200 kHz ($-6dB$ at 120 kHz). For the present experiments, the

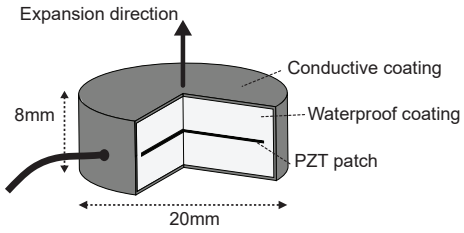

Fig. 1: Embedded piezoelectric transducers designed and manufactured at ULB-BATir

ultrasonic measurement rate has been set to $25 Meas./s$. The duration of each measurement is $3ms$ which allows for a complete attenuation of the ultrasonic wave before the next measurement.

The excitation signal is a low voltage short pulse ($10\ V$, $5\ \mu s$). Such a voltage is very low in comparison to commercial ultrasonic systems which generally involve high voltage (400-800 V) pulsers to increase the signal to noise ratio (SNR) and hence the accuracy of the evaluation of the onset time. This is particularly important for the monitoring of the hardening phase due to the very low amplitude of the recorded signals in fresh concrete. Our approach to increase the SNR for early age monitoring is to benefit from the high measurement rate of our system (which cannot be reached with high-voltage pulsers) and compute the average of one hundred successive measurements. In section 3, one signal consisting of an average of 100 signals measured at a rate of $25 Meas./s$ is recorded every four minutes in order to follow the evolution of the P-wave velocity during the first 70 hours after casting the concrete.

For the bending test, the initial SNR is much better than in fresh concrete: the wave is much less attenuated in hard concrete, so that an average of only ten signals is used. The monitoring is performed continuously at a rate of $25 Meas./s$. Due to the very high measurement rate in this test and the occurrence of damage, some recorded signals are polluted with acoustic emission events which have to be filtered out. Acoustic events are waves generated by the sudden release of energy due to cracking events [34, 35]. In the present study, it was decided to remove these signals from the data. This is not problematic as there are enough non-polluted signals due to the very high measurement rate. Another option would have been to increase the voltage at the emitter side, but this is not the choice made in this study, as explained above. The measurements which are presented in section 4.3 correspond to an average of the last 10 sane signals (i.e. without acoustic emission events). The procedure which is used to detect and remove the polluted signals consists in a cross correlation test with the average of the previous

ten non polluted signals:

$$\mathrm{AE}_j = \frac{\displaystyle\int_0^{t_f} S_j(t)\, S_m(t)\ dt}{\sqrt{\displaystyle\int_0^{t_f} S_j^2(t)\ dt \int_0^{t_f} S_m^2(t)\ dt}} \tag{1}$$

where $S_j(t)$ and $S_m(t)$ are respectively the j^{th} signal and the average of the last ten sane signals. t_f is the measurement time (here 3 ms). This indicator is theoretically equal to 1 for two identical signals. As the measurement rate is much higher than the rate of change due to damage, it can be considered that then successive signals should be almost identical. When an acoustic event occurs, the local cross correlation coefficient drops strongly due to the drastic change of shape of the signal, which allows for discriminating those signals from the sane signals [30]. In practice, because of the inevitable noise on the recorded signals, and the slow evolution of the signal with damage, the indicator is not strictly equal to 1 for a signal without acoustic event so that a threshold has to be considered. We have found that a value of threshold of 0.9 allows for removing all the signals polluted with acoustic emission events. The first ten sane signals are taken when no load is applied to the specimen so that there are no acoustic emission events. The value of AE_j is then computed for each new measurement and if it is sane ($\mathrm{AE}_j > 0.9$), it is included in the stack of the last ten sane signals (see Fig. 3) for averaging.

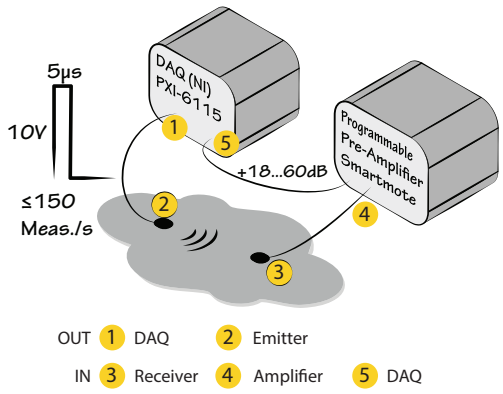

Fig. 2: Fast (≤ 150 ultrasonic measurement per second) and low-voltage (≤ 10 V) data acquisition system. The DAQ is a NI PXI-6115 (out 4 MS/s, in 10 MS/s) and the pre-amplifier is a SMARTMOTE SmartPre. The DAQ and the pre-amplifier (gain) are automatically controlled by a LabView based in-house program.

3. Monitoring of the hardening phase using UPV measurements

The P-Wave velocity is computed from the known distance between the emitter and receiver and the estimated time of flight of the ultrasonic wave. The onset time

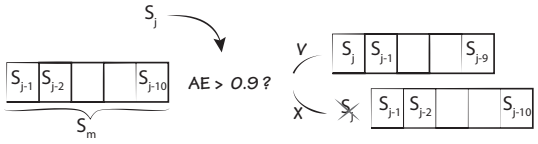

Fig. 3: Process to remove the signals polluted by undesired events such as acoustic emission events: each signal is compared with the average of the last 10 sane signals.

Table 1: Composition of the concrete and geometry of the Non-Reinforced Concrete (Mini) Beams

Geometry of the Non-Reinforced Beam		
$L \times l \times h$	cm	$40 \times 10 \times 10$
Distance between transd.	cm	14.3
Concrete components		Density
CEM I 52.5 N PMES CP2 (Saint Vigor, FR)	kg/m^3	340
Sand 0/4 (Bernières, FR)	kg/m^3	739
Gravel 8/22 (Bernières, FR)	kg/m^3	1072
Total water	kg/m^3	184
Total wet density	kg/m^3	2335
Total dry density	kg/m^3	2250
Mechanical Properties		
Young's Modulus* E_{cm}	GPa	36
Compressive Strength (cube)* $f_{ck,cube}$	MPa	38.04
Compressive Strength (cylinder)* f_{ck}	MPa	30.05
Tensile Strength† f_{ctm}	MPa	$0.3\ f_{ck}^{2/3} = 2.89$
Flexural Strength† $f_{ctm,fl}$	MPa	$(1.6 - \frac{h(m)}{1000})\ f_{ctm} = 4.63$
Expected Maximum Load†	kN	8.1

* Measured
† Estimated from EUROCODE EN 1992-1-1:2004

of the ultrasonic wave can be automatically estimated by finding the minimum of the Akaike Information Criterion (AIC) computed in a given interval (Fig. 5). The AIC is computed as follows:

$$\begin{aligned} \mathrm{AIC}\,(k) = k \log\left(\mathrm{Var}\left(S\ [1,k]\right)\right) + \\ (N-k-1)\log\left(\mathrm{Var}\left(x\,[k+1,N]\right)\right) \end{aligned} \tag{2}$$

where $\mathrm{Var}(X)$ denotes the variance, k is the k^{th} sample of the signal $S(k)$ of length N. This time window is defined around a first estimate of the time of arrival found as a threshold of the amplitude of the envelope of the signal [32, 36]. The envelope function is calculated from the wavelet transform $C(\lambda, \tau)$ [37] of the signal at a low scale (i.e. low frequency) λ

$$C(\lambda,\tau) = \frac{1}{\sqrt{\lambda}} \int_{-\infty}^{\infty} x(t)\overline{\Psi\left(\frac{t-\tau}{\lambda}\right)}dt \tag{3}$$

where the wavelet Ψ is a Complex Gaussian Wavelet.

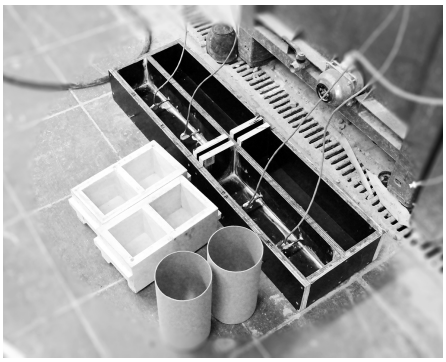

(a) Two pairs of embedded piezoelectric transducers are set in two non-reinforced concrete beams.

(b) Zoom on the embedded transducers

Fig. 4: Specimens used in the study. The concrete property and the geometry of the beams are given in Table 1.

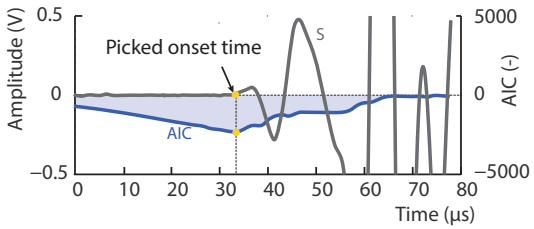

Fig. 5: Estimation of the onset time with the AIC.

The different devices of the monitoring system and the layers surrounding the transducers necessarily result in a certain time delay in the sensor-actuator line so that the system should be calibrated for accurately determining the time-of-flight between the sensor and the actuator. This is performed by measuring the travel time in water [28], where the wave velocity is accurately known.

Knowing the distance between the emitter and the receiver and the delay, the veloc-

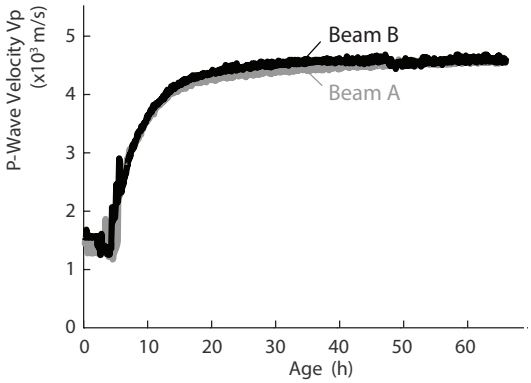

Fig. 6: Evolution of the P-Wave Velocity as a function of the time since casting.

ity of the fastest wave (the P-wave) can be deduced. Fig. 6 shows the evolution of the P-Wave velocity during the first 70 hours after casting the concrete. It can be observed that the typical S-Curve which describes the hydration kinetics is well caught by the monitoring system from very early age.

The dynamic E-modulus can therefore be deduced from the P-Wave velocity [38]:

$$E_{dyn} = \rho V_P^2 \frac{\left(1 + \nu_{dyn}\right)\left(1 - 2\nu_{dyn}\right)}{\left(1 - \nu_{dyn}\right)} \tag{4}$$

Assuming a value of the dynamic Poisson's ratio of $\nu_{dyn} \approx 0.3$ at 28 days [38], the dynamic E-modulus is 36 GPa.

4. Long term damage monitoring

A three-points bending test is performed on one of the two non-reinforced concrete beams after 28 days. An overview of the test setup is shown on Fig. 7. The loading machine is a 200 kN hydraulic jack bending testing machine. The force and the displacement have been recorded on a computer using a National Instruments DAQ system (`NI PXI-4461`). The vertical displacement at the center of the beam is measured by an inductive displacement transducer (±5 mm LVDT, HBM W5TK) wired to the DAQ through a specific signal conditioner. The ultrasonic monitoring system is described on Fig. 2. During the bending test, short low voltage pulses are sent at regular interval (5 μs, 10 V, 25 $Signals/s$).

4.1. Loading Procedure

Since the beam is not reinforced, the maximum load which can be applied is reached at the initiation of the crack. The loading machine is controlled in displacement thanks to an inductive linear displacement transducer (LVDT) as shown in Fig. 7.

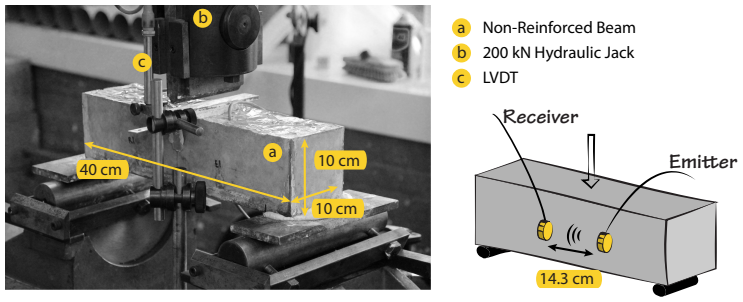

Fig. 7: Overview of the test setup for the bending test. The geometry of the specimen is given in Table 1. The loading machine is a 200 *kN* hydraulic jack bending testing machine.

In order to make sure that the crack is initiating at the center of the beam, a notch of 1 *cm* of depth is sawed (Fig. 8). The loading procedure and the force-displacement curve are displayed on Fig. 8 where different pictures allow to track the crack opening. The beam is unloaded right after the crack visually appears. The different pictures are numbered (from **1** to **3**) in order to relate them to a) the force-displacement and force-time curves on Fig. 8, b) the relative velocity variation displayed on Fig. 10, and c) the evolution of the damage index on Fig. 13. The crack visually appears when the maximum load is already exceeded (see **2** in Fig. 8). It is important to note that the sudden load decreases which can be observed in the loading phase are due to technical features of the loading machine.

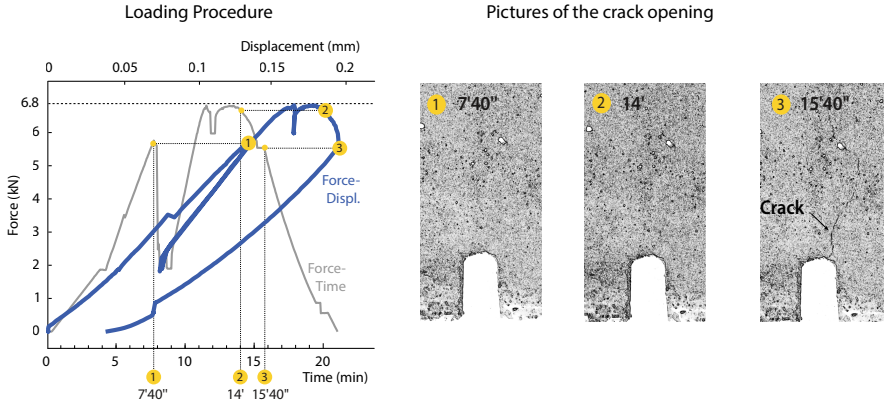

Fig. 8: Loading Procedure and Force-Displacement curve related to the visual appearance of the crack. The three point bending test is controlled in displacement using a LVDT.

4.2. UPV measurements

When in service, a concrete structure is subject to operational variability due to changing loads (traffic, wind, ...) and environmental effects (temperature, humidity).

It is known that the wave velocity varies to a certain extent due to these changing conditions, as well as due to the damage. These relative velocity changes are very small compared to the changes of velocities at the early age. In this paper, we explore and compare different methods to estimate in real time the relative wave velocity variation using embedded piezoelectric transducers with the focus on the efficiency to monitor very small changes of velocities :

I) The first method consists in estimating the onset time of the received wave (UPV) as described in section 3. Considering a small variation of the velocity, the relative velocity change is therefore given by

$$\epsilon = \frac{\delta V}{V_0} \approx -\frac{\delta t_r}{t_{r,0}} = -\frac{t_r - t_{r,0}}{t_{r,0}} \tag{5}$$

where t_r and $t_{r,0}$ are respectively the onset time of the current signal $S(t)$ and the onset time of the baseline signal $S_0(t)$. It is known that the direct evaluation of the time of flight leads to high uncertainties as it clearly appears in the experiments presented hereafter (Fig. 10). The precision of ϵ depends directly on the sampling rate of the measurement ($10MHz$ in the present case).

II) The second method is based on the classical coda wave interferometry (CWI) method. This method is known to be very precise to track small velocity variations due to the temperature effects or small stress variations (acoustoelastic effect). The total wave field is simply the summation of all the waves that propagate along all the possible paths. One can therefore describe a multiply scattered wave $S(t)$ as the superposition of the different components of an initial wave packet with random amplitudes and delays. Consequently, the effect of a global velocity change $\epsilon = dV/V$ in the medium is to stretch the original signal $S_0(t)$. The stretching factor ϵ is determined by searching for the maximum cross-correlation coefficient $CC(\epsilon)$ in all the duration of the CODA (see Fig. 9)

$$\mathrm{CC}(\epsilon) = \frac{\int_{t_0}^{t_f} S(t)\, S_0\Big(t(1+\epsilon)\Big)\, dt}{\sqrt{\int_{t_0}^{t_f} S^2(t)\ dt \int_{t_0}^{t_f} S_0^2\Big(t(1+\epsilon)\Big)\, dt}} \tag{6}$$

where t_0 and t_f depend on the time window in which the cross correlation is estimated. The strategy which is adopted is to use the MATLAB optimization function *fminbnd* to find the minimum value of the decorrelation factor ($DC = 1-CC$). When the maximum correlation is high, ϵ can directly be used as an estimate of the relative wave velocity change. This will only be the case if the velocity change is uniform in a large area around the transducers. The extent of this area depends mainly on the time of arrival of the latest waves which have travelled a much longer path and potentially reached much more distant locations than the area around the transducers. In most practical applications, the stress field and environmental parameters are not uniform in such a large area, so that the method is not applicable.

III) As an alternative, the third method, which is introduced in the present study, is directly inspired by the CWI, but it is applied on the direct wave instead of the CODA (see Fig. 9). The introduction of the direct wave interferometry (DWI) is motivated by the fact that this part of the wave is mainly impacted by variations in a restricted area located along the line of sight from the source to the receiver [39–41]. In such a restricted area, it is expected that the wave velocity changes will be almost uniform, making the measurement robust to complex loading conditions and effects of boundary conditions. The use of a shorter wave will result in a lower resolution than CWI because the delays in the early part of the signal are smaller than the delays in the CODA.

The initial (t_i) and final times (t_f) used for the computation of the correlation coefficient CC for CWI and DWI are shown in Fig. 9. For CWI, we consider that the wave path should be longer than several (at least 2 or 3) times the elastic mean free path l_s (the distance between successive scattering events, see [41]). For concrete the elastic mean free path l_s is usually around 15 to 20 cm at 200 kHz [12, 42]. For a wave velocity of 4500 m/s, $3l_s$ corresponds to a time of flight of 133μs. For DWI, t_f is based on the observation that before that instant, signals are not changing before cracking occurs. At that time, the wave has only encountered a few scattering events. Further investigations are needed in order to link this value to an intrinsic measure which should be related to the stress gradients and relative positions of boundary conditions, but this is outside of the scope of the present study.

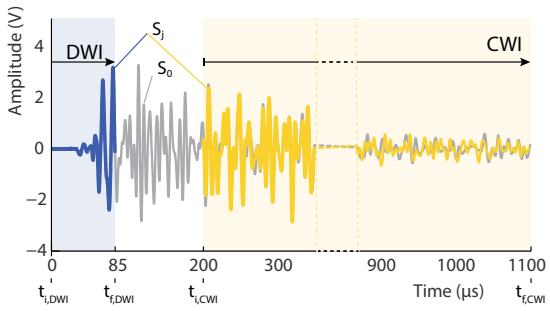

Fig. 9: Snapshot of a signal and definition of the time windows used for the CWI and the DWI methods in the case of the bending test.

The evolution of the relative wave velocity change during the three-point bending test is shown in Fig. 10 using the three methods. The line corresponding to the direct measurement of the TOF is obtained by denoising (wden in MATLAB) the values actually found. One can observe that

(a) the direct estimation of the relative velocity variation from the TOF leads to very noisy results. In particular, one can observe that the resolution is constrained by the sampling rate of the measured wave (see the individual dots corresponding to the actual measurements in Fig. 10). Before denoising, the accuracy of the relative wave velocity change is in the order of 2% (2.10^{-2}). After denoising, the resolution is improved and reaches about 2.10^{-3}.

(b) the resolution of CWI is about 2.10^{-5}, as can be estimated from Fig. 10 (bottom). The later result is in accordance with the findings in [9]. Fig. 11 shows however that for CWI, the wave starts to be decorrelated from the baseline after a time of approximately 3 minutes. When the signal is decorrelated, time stretching will fail to give a physical value of the relative wave velocity variation. CWI clearly fails to catch the strong velocity variations due to damage after 10 minutes while these are obvious from the TOF measurements.

(c) the resolution of DWI is about 2.10^{-4}. The decorrelation starts to increase around 11 minutes which corresponds to the time of the initiation of the crack. The technique can therefore be used with confidence before damage appears to track small relative wave velocity changes, with an accuracy which is a compromise between TOF and CWI. When damage occurs, the velocity changes seem to be slightly underestimated by DWI due to the decorrelation.

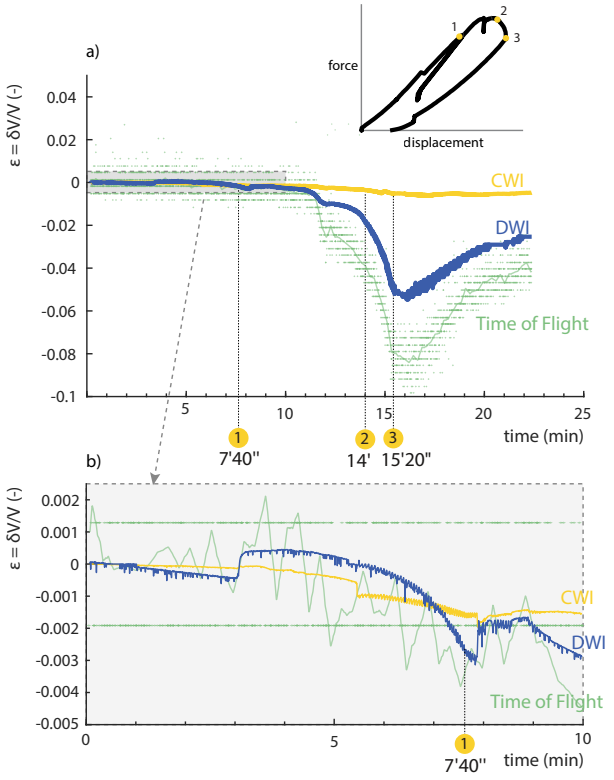

Fig. 10: Evolution of the relative velocity change as function of the time (bending test). The 'time of flight' line is obtained by denoising (wden in MATLAB) the actual measurements (green dots).

The decorrelation coefficient is a clear indicator that the shape of the wave has changed, in which case, the value of the time stretching (and therefore the wave velocity change) is not reliable. When wave velocity changes in the media are uniform,

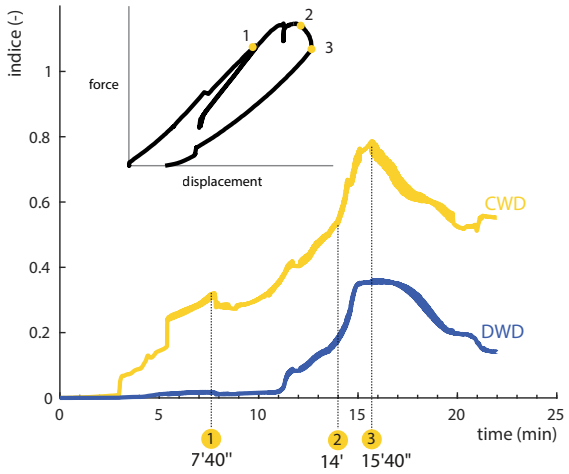

Fig. 11: Evolution of the decorrelation as function of the time (bending test).

time stretching gives a reliable estimate of the wave velocity change. In our tests, we see that when using CWI, the wave shape is altered well before damage occurs. The CODA contains wave packets which have travelled in the whole concrete specimen. As the stress state is not uniform due to the nature of the test (bending), the acoustoelastic effect will have a non-uniform impact on the CODA, resulting in a decorrelation. Other factors such as stress concentration in the areas close to the boundary conditions have a similar effect. When using DWI, the wave that is recorded and used to compute the decorrelation has only travelled in a restricted area around the transducers, and we notice that the correlation is very good before the damage occurs. As the damage induces a local change of wave velocity between the transducers, the decorrelation starts to increase with its appearance.

One can conclude that before the damage occurs, DWI can be used with confidence to track accurately very small (up to 0.3 % in our test) velocity changes. We believe that these velocity changes are mainly due to the acoustoelastic effects. The focus of this paper is however not to understand deeply where these changes are coming from, but to propose a method to filter out their effects.

4.3. Damage monitoring under changing operational conditions

For real-time monitoring, it is important to be able to distinguish between the effects of damage and operational conditions. As the wave velocity varies due to the appearance of damage as well as changing operational conditions, it is not a robust indicator of damage. The previously used damage indicator, the early wave damage index, has also been shown to be sensitive to operational conditions [30]. In this paper, we propose to apply time stretching with DWI in order to filter out operational conditions before computing the damage index.

The time-of-flight and the first wave amplitude are known to be sensitive to cracking. We have therefore proposed in [29] to define a damage indicator which focuses on the early wave in the signal. This damage indicator has been used to monitor cracking in different laboratory setups consisting in: **(i)** three points bending tests on concrete beams [29, 31], **(ii)** pull-out tests on an anchorage in a large concrete block [29, 33], **(iii)** compression tests on a cylinder [30].

For **(i)** and **(ii)**, the results have shown the excellent sensitivity of the damage indicator to the onset of cracking, the indicator is able to detect damage before cracks are visible on the outer surface. For **(iii)**, we have found that because of the higher levels of stresses involved in compression tests, the acoustoelastic effect [10] was affecting the damage index. An alternative indicator was therefore proposed which consists in monitoring the change of amplitude of the first peak only. In much the same way, we propose here to apply the damage index on the stretched rather than the initial signal using the time stretching technique described in Section 4.2. This allows to get rid of the sensitivity to the change of the wave velocity and focus on the change of amplitude and shape of the first peak. The damage index DI is now expressed as

$$\mathrm{DI}_j = \sqrt{\frac{\int_{t_1}^{t_2} \left(S_j\left(t\,(1-\epsilon_{max})\right) - S_0\,(t)\right)^2 \, dt}{\int_{t_1}^{t_2} S_0^2\,(t) \, dt}} \tag{7}$$

where $S_j(t)$ corresponds to the amplitude of the damaged signal, $S_0(t)$ is the amplitude of the healthy signal, t_1 is the time of arrival of S_0, and $t_2 - t_1$ corresponds to the duration of the first half-period. This is represented on Fig. 12 where an example of a healthy and a signal with cracking are presented. ϵ_{max} corresponds to the value of time stretching which maximizes the correlation coefficient CC defined in (6).

Fig. 13 shows that if no time stretching is applied to the measured signals, the DI is affected by these small velocity changes (see the small increase of the DI around point 1 which corresponds to the time when the velocity change is the highest according to the DWI time stretching presented in Fig. 10). Applying time stretching allows to get rid of the small velocity changes due to operational perturbations, at the cost of a slightly lower sensitivity to the damage.

In Fig. 14 we compare the DI corrected with time stretching to the evolution of the amplitude of the first peak of the wave previously proposed in [30] as a damage indicator robust to environmental factors such as the acoustoelastic effect. As the figure shows, the two approaches lead to very similar results. The choice between one or the other should be mainly dictated by the computational efforts involved for the computation of each indicator.

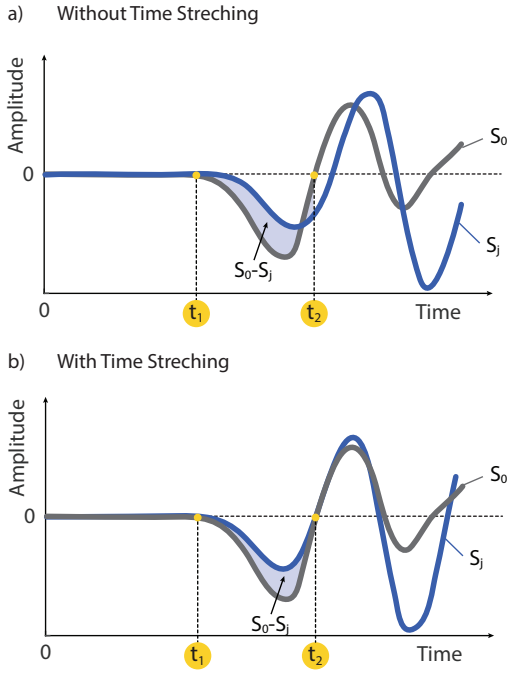

Fig. 12: Example of a healthy and a damaged signal and definition of the quantities used for the computation of the damage index (with and without time stretching).

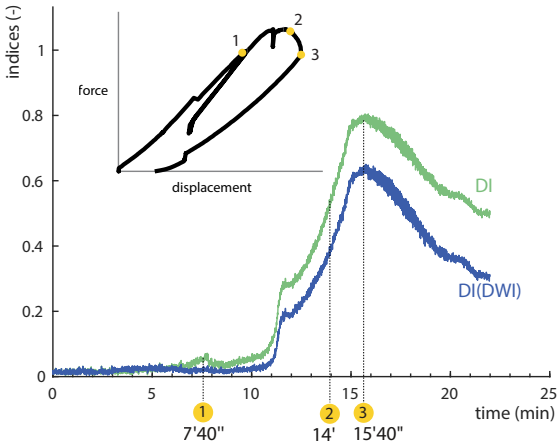

Fig. 13: Evolution of the damage indicator as function of the time (DWD: direct wave decorrelation, CWD: coda wave decorrelation).

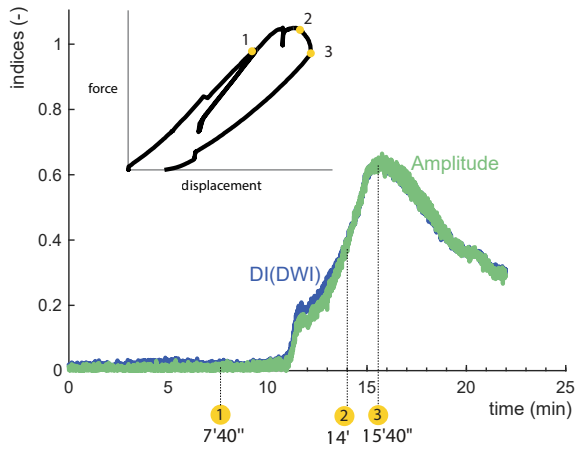

Fig. 14: Evolution of the damage indicator, and the first peak amplitude as function of the time (bending test).

5. Conclusions

This paper presented a methodology for lifelong monitoring of concrete structures. The technique is based on the use of pairs of low-cost piezoelectric transducers which are embedded inside the concrete structure during the construction phase. A high-frequency pulse is sent to the emitter and the receiver records the wave after propagation. Based on the recorded signals at regular time intervals, information about the state of the microstructure of concrete can be obtained. The efficiency of the method has been demonstrated through laboratory tests on two small concrete beam specimen.

At early age, we have shown that it was possible to track the *P*-wave velocity change from the liquid to the solid state, and to use it to estimate the evolution of mechanical properties in real-time. For long-term monitoring, we have tested one of the sample beams under a three-point bending test in order to induce progressive cracking in the middle of the beam. Three different techniques were analyzed in order to track small relative velocity changes. The time of flight has a low resolution (around 1%) which can be improved to 0.1% with denoising if the number of measurements is sufficient. The CWI approach has been shown to be too sensitive to the non-uniform stress field and effects of boundary conditions in the test. While its accuracy is very high (around 2.10^{-5}), it is not applicable for in-situ monitoring of the wave velocity changes on real structures. As it is focused only on the early wave arrive, the DWI has a slightly lower accuracy (around 2.10^{-4}) but is much more robust with respect to the loading conditions and changing boundary conditions. We have shown that it is able to track accurately small velocity changes before the damage appears.

DWI can therefore be used to stretch the recorded signals and correct for small wave velocity changes due to operational conditions. Based on this finding, we have

defined a damage indicator which is made robust to operational changes thanks to time stretching using DWI. The velocity changes in our tests are thought to be due to the effect of applied stresses (only acoustoelastic effect), and not to environmental factors such as temperature or humidity. The applicability of the technique in changing environmental conditions remains to be tested, but as environmental changes are likely to produce more or less uniform changes of material properties, the velocity changes are also likely to be uniform so that time stretching is applicable to compensate for these effects and differentiate them from cracking.

In our test, the corrected damage indicator is able to track efficiently the appearance of damage while being insensitive to changing operational conditions. The results obtained have been compared to the previously proposed damage indicator based on the first peak amplitude, which shows very similar results. Both approaches are therefore seen as very efficient for automated long term monitoring of cracking in concrete structures using embedded piezoelectric transducers.

One important issue which needs further investigation is the a priori determination of the final time t_f to be used in DWI in order not to be sensitive to changing boundary conditions and non-uniform stress fields. This will be investigated in more details in the future.

Acknowledgments

This study was supported by the Belgian National Fund for Scientific Research (FRS-FNRS) and by the Fonds David et Alice Van Buuren.

References

[1] Saul, A.. Principles underlying the steam curing of concrete at atmospheric pressure. Magazine of Concrete Research 1951;6(2):127–140.

[2] Yikici, T., Chen, H.. Use of maturity method to estimate compressive strength of mass concrete. Construction and Building Materials 2015;(95):802–812.

[3] EN 12504-4:2004 (E), . Testing concrete. Determination of ultrasonic pulse velocity. European Standard 2004;.

[4] ASTM C597, . Standard Test Method for Pulse Velocity Through Concrete. American Society for Testing and Materials, West Conshohocken, PA, USA 2016;:1–4doi:10.1520/C0597-09.

[5] Saint-Pierre, F., Philibert, A., Giroux, B., Rivard, P.. Concrete quality designation based on ultrasonic pulse velocity. Construction and Building Materials 2016;(125):1022–1027.

[6] BS 1881 - part 203, . Testing concrete. Recommendations for measurement of velocity of ultrasonic pulses in concrete. British Standard 1986;.

[7] Carette, J., Staquet, S.. Monitoring the setting process of eco-binders by ultrasonic p-wave and s-wave transmission velocity measurement: Mortar vs concrete. Construction and Building Materials 2016;(94):32–41.

[8] Bogas, J., Gomes, M., Gomes, A.. Compressive strength evaluation of structural lightweight concrete by non-destructive ultrasonic pulse velocity method. Ultrasonics 2013;(53):962–972.

[9] Larose, E., Hall, S.. Monitoring stress related velocity variation in concrete with a 2 x 10(-5) relative resolution using diffuse ultrasound. The Journal of the Acoustical Society of America 2009;125(4):1853–6. doi:10.1121/1.3079771.

[10] Lillamand, I., Chaix, J.F., Ploix, M.A., Garnier, V.. Acoustoelastic effect in concrete material under uni-axial compressive loading. NDT & E International 2010;43(8):655–660. doi:10.1016/j.ndteint.2010.07.001.

[11] Larose, E., Obermann, A., Digulescu, A., Planès, T., Chaix, J.F., Mazerolle, F., et al. Locating and characterizing a crack in concrete with diffuse ultrasound: A four-point bending test. The Journal of the Acoustical Society of America 2015;138(1):232–241. doi:10.1121/1.4922330.

[12] Zhang, Y., Planès, T., Larose, E., Obermann, A., Rospars, C., Moreau, G.. Diffuse ultrasound monitoring of stress and damage development on a 15-ton concrete beam. The Journal of the Acoustical Society of America 2016;139(4):1691–1701. doi:10.1121/1.4945097.

[13] Frojd, P., Ulriksen, P.. Continuous wave measurements in a network of transducers for structural health monitoring of a large concrete floor slab. Structural Health Monitoring 2016;15(4):403–412. doi:10.1177/1475921716642139.

[14] Qin, L., Li, Z.. Monitoring of cement hydration using embedded piezoelectric transducers. Smart Mater Struct 2008;17. 055005.

[15] Kong, Q., Hou, S., Ji, Q., Mo, Y., Song, G.. Very early age concrete hydration characterization monitoring using piezoceramic based smart aggregates. Smart Mater Struct 2013;22. 085025.

[16] Gu, H., Song, G., Dhonde, H., Mo, Y., Yan, S.. Concrete early-age strength monitoring using embedded piezoelectric transducers. Smart Mater Struct 2006;15:1837–1845.

[17] Dansheng, W., Hongping, Z.. Monitoring of strength gain of concrete using embedded PZT impedance transducer. Construction and Building Materials 2011;25:3703–3708.

[18] Song, G., Gu, H., Mo, Y., Hsu, T., Dhonde, H.. Concrete structural health monitoring using embedded piezoceramic transducers. Smart Mater Struct 2007;16:959–968.

[19] Zhao, X., Li, H., Du, D., Wang, J.. Concrete structure monitoring based on built-in piezoelectric ceramic transducers. Proc of SPIE Vol 6932, 693208 2008;.

[20] Annamdas, V., Yang, Y., Soh, C.. Impedance based concrete monitoring using embedded PZT sensors. Int J Civil and Struct Engng 2010;1(3):414–424.

[21] Liao, W., Wang, J., Song, G., Gu, H., Olmi, C., Mo, Y., et al. Structural health monitoring of concrete columns subjected to seismic excitations using piezoceramic-based sensors. Smart Mater Struct 2011;20. 125015.

[22] Feng, Q., Kong, Q., Huo, L., Song, G.. Crack detection and leakage monitoring on reinforced concrete pipe. Smart Mater Struct 2015;24. 115020.

[23] Zou, D., Liu, T., Huang, Y., Zhang, F., Du, C., Li, B.. Feasibility of water seepage monitoring in concrete with embedded smart aggregates by P-wave travel time measurement. Smart Mater Struct 2014;23. 067003.

[24] Kong, Q., Feng, Q., Song, G.. Water presence detection in a concrete crack using smart aggregates. Int J of Smart and Nano Mat 2015;6(3):149–161.

[25] Liu, T., Huang, Y., Zou, D., Teng, J., Li, B.. Exploratory study on water seepage monitoring of concrete structures using piezoceramic based smart aggregates. Smart Materials and Structures 2013;22(6):065002. doi:10.1088/0964-1726/22/6/065002.

[26] Li, Z., Qin, L., Huang, S.. Embedded piezo-transducer in concrete for property diagnosis. Journal of Materials in Civil Engineering 2009;21(11). 085025.

[27] Liu, T., Zou, D., Du, C., Wang, Y.. Influence of axial loads on the health monitoring of concrete structures using embedded piezoelectric transducers. Structural Health Monitoring 2017;16(2):202–214. doi:10.1177/1475921716670573.

[28] Dumoulin, C., Karaiskos, G., Carette, J., Staquet, S., Deraemaeker, A.. Monitoring of the ultrasonic P-wave velocity in early-age concrete with embedded piezoelectric transducers. Smart Materials and Structures 2012;21(4):047001. doi:10.1088/0964-1726/21/4/047001.

[29] Dumoulin, C., Karaiskos, G., Sener, J.Y., Deraemaeker, A.. Online monitoring of cracking in concrete structures using embedded piezoelectric transducers. Smart Materials and Structures 2014;23(11):115016. doi:10.1088/0964-1726/23/11/115016.

[30] Dumoulin, C., Deraemaeker, A.. Real-time fast ultrasonic monitoring of concrete cracking using embedded piezoelectric transducers. Smart Materials and Structures 2017;26(10):104006. doi:10.1088/1361-665X/aa765e.

[31] Dumoulin, C., Karaiskos, G., Deraemaeker, A.. 8 - Monitoring of crack propagation in reinforced concrete beams using embedded piezoelectric transducers. In: Ohtsu, M., editor. Acoustic Emission and Related Non-Destructive Evaluation Techniques in the Fracture Mechanics of Concrete. Woodhead Publishing

Series in Civil and Structural Engineering; Oxford: Woodhead Publishing. ISBN 978-1-78242-327-0; 2015, p. 161–175. doi:10.1016/B978-1-78242-327-0.00008-8.

[32] Dumoulin, C., Deraemaeker, A.. Design optimization of embedded ultrasonic transducers for concrete structures assessment. Ultrasonics 2017;79:18–33. doi:10.1016/j.ultras.2017.04.002.

[33] Dumoulin, C., Karaiskos, G., Deraemaeker, A.. Concrete Monitoring Using Embedded Piezoelectric Transducers. In: Beer, M., I.A., K., Patelli, E., Au, I.K., editors. Encyclopedia of Earthquake Engineering; 1 ed. Berlin, Heidelberg: Springer Berlin Heidelberg. ISBN 978-3-642-35345-1; 2015, p. 1–12. doi:10.1007/978-3-642-36197-5_94-1.

[34] Ohtsu, M., editor. Acoustic Emission and Related Non-Destructive Evaluation Techniques in the Fracture Mechanics of Concrete: Fundamentals and Applications. Woodhead Publishing Series in Civil and Structural Engineering: Number 57; Cambridge: Elsevier; 2015. ISBN 9781782423270. doi:10.1016/B978-1-78242-327-0.01001-1.

[35] Grosse, C., Ohtsu, M.. Acoustic Emission Testing. Berlin, Heidelberg: Springer Berlin Heidelberg; 2008. ISBN 978-3-540-69895-1. doi:10.1007/978-3-540-69972-9.

[36] Kurz, J.H., Grosse, C.U., Reinhardt, H.W.. Strategies for reliable automatic onset time picking of acoustic emissions and of ultrasound signals in concrete. Ultrasonics 2005;43(7):538–46. doi:10.1016/j.ultras.2004.12.005.

[37] Daubechies, I.. Ten Lectures on Wavelets. Society for Industrial and Applied Mathematics; 1992. ISBN 978-0-89871-274-2. doi:10.1137/1.9781611970104.

[38] Delsaute, B., Boulay, C., Granja, J., Carette, J., Azenha, M., Dumoulin, C., et al. Testing Concrete E-modulus at Very Early Ages Through Several Techniques: An Inter-laboratory Comparison. Strain 2016;52(2):91–109. doi:10.1111/str.12172.

[39] Dumoulin, C., Deraemaeker, A.. From early age assessment of concrete properties to crack detection using embedded ultrasonic transducers. In: 2nd International RILEM/COST Conference on Early Age Cracking and Serviceability in Cement-based Materials and Structures - EAC2; vol. 1. Brussels (Belgium): RILEM; 2017, p. 137–142.

[40] Snieder, R., Scales, J.. Time-reversed imaging as a diagnostic of wave and particle chaos. Physical Review E 1998;58(5):5668–5675. doi:10.1103/PhysRevE.58.5668.

[41] Tourin, A., Fink, M., Derode, A.. Multiple scattering of sound. Waves in Random Media 2000;10(4):R31–R60. doi:10.1088/0959-7174/10/4/201.

[42] Schurr, D.P., Kim, J.Y., Sabra, K.G., Jacobs, L.J.. Damage detection in concrete using coda wave interferometry. NDT & E International 2011;44(8):728–735. doi:10.1016/j.ndteint.2011.07.009.